scientific reports

Check for updates

OPEN

Enhancement of the catalytic performance of Co-ZIF/WO_3 heterostructures for selective catalytic reduction of NO_x

Hassan Alamgholiloo[1], Esrafil Asgari[1✉], Amir Sheikhmohammadi[1✉], Naser Ghasemian[2✉], Bayram Hashemzadeh[1] & Heshmatollah Nourmoradi[3,4]

Nitrogen oxides (NOx) are one of the growing air pollutants in industrial countries, and their emissions are regulated by stringent legislation. Therefore, the design of the catalyst comprised of metal oxides and ZIFs a potential solution for improving selective catalytic reduction (SCR) of NOx. Here, an efficient strategy was described to fabricate Co-ZIF/WO_3 heterostructures for SCR of NOx. First, WO_3 nanostructures were fabricated by the solvothermal method, and subsequently epitaxial growth of ZIF-67 on the metal oxide surface to create a new type of semiconductor Co-ZIF/WO_3 heterostructures. The obtained heterostructures were systemically characterized by wide-angle XRD, FESEM, UV DRS, FT-IR, AFM, and TEM spectroscopies. The Co-ZIF/WO_3 heterostructures shift the temperature corresponding to the maximum conversion around 50 °C towards lower temperatures. The maximum conversion is substantially enhanced from 55% at 400 °C to 78% at 350 °C. The enhanced activity is attributed to better interaction and synergic effect of WO_3 incorporated into ZIF-67 and also the electron transfer facility between the WO_3 and Co species in Co-ZIF/WO_3 heterostructures. Moreover, Co-ZIF/WO_3 results in a distinct effect on the production of carbon monoxide (CO) in the product gas stream. The current study highlights some of the challenges in the development of semiconductor-based heterostructures for a decrease in air pollution.

Keywords SCR-NOx, Propane, Heterostructure, Co-ZIF/WO_3

Combustion of fossil fuels and burning of biomass has caused air pollution and environmental, creating health problems in the world[1–4]. Therefore, the issue of air pollution has seriously affected people's ability to have a better life[2,5]. Nitrogen oxides ($NO_2 + NO = NOx$) as one of the air pollutants play a vital role in tropospheric chemistry such as ozone formation, production of secondary aerosols, and acid rain[6,7]. NOx pollutants are increasingly produced from a variety of human activities and natural resources[7]. Among NOx gases, NO_2 has the highest concentration in the ambient air and can be fatal if inhaled in large quantities[8]. Furthermore, this poisonous gas has a reddish-brown color with a boiling point of 21.1 °C and low partial pressure that keeps it gaseous[8,9]. Also, this corrosive gas has a strong oxidant and physiologically stimulates the lower respiratory tract and thereby is toxic to humans[9]. Most atmospheric NO_2 is released as NO, which is rapidly oxidized by ozone to NO_2. Also, NOx gases can combine with common organic matter and even ozone to form a wide range of toxic compounds, which can cause mutations in DNA[10,11]. In addition, NOx can cause serious respiratory problems, odor disorders, fatigue, throat irritation, nerve disorders, and increased acute bronchitis in humans[12,13]. Consequently, developing an efficient method for the complete removal of NOx has become a global priority.

Recently, different methods have been expanded to control these gaseous pollutants, including thermal[14], adsorption[15], and catalytic[16,17] methods due to the importance of this pollutant in the environment. In the thermal method, a high temperature is used to decompose NO, which high temperature causes undesirable side reactions[14]. In the adsorption method, the efficiency of the adsorbent is reduced due to the adsorption of NOx on its active surface[18]. Therefore, these two methods are not suitable for NOx removal. Recently, many

[1]Department of Environmental Health Engineering, School of Health, Khoy University of Medical Sciences, Khoy, Iran. [2]Department of Chemical Engineering, University of Bonab, Bonab, Iran. [3]Health and Environment Research Center, Ilam University of Medical Sciences, Ilam, Iran. [4]Department of Environmental Health Engineering, School of Health, Ilam University of Medical Sciences, Ilam, Iran. ✉email: esrafil_asgari@khoyums.ac.ir; a_sheikhmohammadi@khoyums.ac.ir; n.ghasemian@gmail.com

investigate have reported the efficient method of selective catalytic reduction (SCR) for NOx abatement via different hydrocarbon compounds such as propane[19,20], methane[21], and ammoniac as a reductant. Moreover, semiconductor materials with different charge migration pathways have been used in an industrial SCR system[22]. WO_3-based materials as efficient semiconductors have been considered to be a promising photocatalyst in abating NOx emissions from air pollution[23]. Unfortunately, the low electrical conductivity and negligible specific surface area have restricted the performance of pure WO_3 in the SCR-NOx-Propane process. Fortunately, the conjugation of this semiconductor material with Zeolites could improve light harvesting and charge separation for the removal of NOx[24]. Zeolites such as ZSM-5[25], clinoptilolite[26], and metal oxides including cerium oxide[27], zirconium oxide[28], vanadium oxide[29], and tungsten oxide[23] have been proposed as catalysts for the removal of NO_x with various methodologies. Recently, Lee et al. developed CuSn/ZSM-5 for the HC-SCR-NOx process[30]. Moreover, the effect of the addition of molybdenum on the enhanced low-temperature SCR of NOx by NH_3 over $MnOx/\gamma\text{-}Al_2O_3$ catalysts was investigated by Yang and et al.[31]. Furthermore, Zhan et al. reported mesoporous WO_3 for SCR-NOx with NH_3[32]. Recently, our research team developed engineered nanostructures to expand the photo-based advanced oxidation process (AOP)[33–36] and persulfate-based AOP[4,37–39] for the removal of organic contaminations from wastewater.

Zeolitic imidazolate frameworks (ZIFs) with the advantages of uniform pore size and high BET surface have been used as catalysts for selective catalytic reductions (SCR)[40,41]. Recently, ZIF-based materials like ZIF-67 have been utilized as an efficient microporous for NO_x abatement and its performance in the SCR-NOx process has been investigated[42]. Recently, Zhao et al. reported Cu-ZIF performance on NH_3-SCR-NOx[42]. Moreover, the performance of Co_3O_4-PC derived from ZIF-67 for low-temperature SCR of NOx by ammonia was studied by Bai et al.[42]. However, the activity of ZIF-67 on propane-SCR-NOx has not been studied so far. Therefore, the activity of ZIF 67 as an efficient catalyst for NOx abetment is investigated. In this study, we have attempted to develop an efficient nanostructure for promoting the activity of WO_3 as a conventional catalyst for NOx abatement. Accordingly, a porous nanocomposite of Co-ZIF/WO_3 due to the better interaction and synergic effect of WO_3 nanostructure incorporated into ZIF-67 was used. Also, the electron transfer facility between the WO_3 and Co species in the channels of Co-ZIF/WO_3 exhibited a lower energy band gap of Co-ZIF/WO_3 led to enhancing the catalytic activity of Co-ZIF/WO_3 in the NOx process. Therefore, a part of the study belongs to the design, fabrication, and characterization of nanocomposite of Co-ZIF/WO_3 heterostructure and another part belongs to the performance of WO_3, ZIF-67, and Co-ZIF/WO_3 in conversion and temperature on propane-SCR-NOx. According to the latest findings reported, there is no study on the design of Co-ZIF/WO_3 nanocomposite for selective catalytic reduction (SCR) of NOx. Therefore, the current study provided a rational design for a decrease in air pollution.

Experimental

Material

Tungstate dihydrate ($Na_2WO_4{\cdot}2H_2O$), cobalt nitrate hexahydrate ($Co(NO_3)_2{\cdot}6H_2O$), 2-methylimidazole (MeIM), polyvinylpyrrolidone (PVP), oxalic acid ($C_2H_2O_4$) were purchased from Sigma-Aldrich Co (USA) and and Merck Co. (Germany). Furthermore, hydrochloric acid (HCl), methanol (MeOH), ethanol (EtOH), and other solvents were used without further purification.

Characterization

The characterization of as-prepared nanostructures and catalytic reduction of NO_x is described in text S1 of supplementry Information.

Fabrication of WO_3 nanoplates

The WO_3 nanostructure was prepared following a method described by Zheng and co-workers[43]. In a typical experiment, 8.25 g $Na_2WO_4{\cdot}2H_2O$ was dissolved in 25 mL dionized water under sonication. Subsequently, 2.0 mL of 2.0 M HCl was added to the mixture reaction and then oxalic acid was added to the mixture to adjust the final pH value to approximately 2.50 and diluted to 250 mL. After that, 1.17 g NaCl was added to the mixture reaction under sonication. After 10 min sonication, 70 mL of the above precursor solution was transferred into a 100 mL of Teflon-lined autoclave and heated for 4.0 h at 170 °C. After completion of the reaction, the resulting yellow precipitate was washed several times with DI-H_2O and EtOH for purification to obtain the final WO_3 nanoplates.

Fabrication of Co-ZIF/WO_3 heterostructure

To fabricate Co-ZIF/WO_3 heterostructures, firstly 0.20 g of as-synthesized WO_3 with 2.0 mmol PVP as structure-director agents was dispersed in 100 mL MeOH under sonication. Subsequently, 1.05 g of $Co(NO_3)_2{\cdot}6H_2O$ was added to the mixture reaction shaken vigorously for 15 min. Afterward, 6.15 g 2-MeIM was added to the mixture reaction under stirring for 24 h to grow ZIF-67 microcrystals on the WO_3 surface. Finally, the prepared precipitates were separated by centrifugation and washed with MeOH several times, and dried at 80 °C under a vacuum. The schematic fabrication of the Co-ZIF/WO_3 heterostructure is revealed in Fig. 1.

Investigation of catalytic activity

The schematic catalytic reactor system used in this study was displayed in Fig. 2. In brief, the inlet gas mixture involved nitric oxide (30 mg/L), nitrogen dioxide (460 mg/L), oxygen (2.5 vol%), C_3H_8 (1.0 g/L), and also argon gas (balance) was introduced to the flow meter set at 300 mL/min. Afterward, the gas mixture was preheated and also conducted in an integral reactor containing 0.50 g of the catalyst. A stainless steel vessel was used as a reactor with a diameter of 0.50 inches. An electrical furnace was applied to heat the reactor. Various thermocouples at the inlet, inside the reactor bed, and outlet of the stream were employed to control system temperature. This system

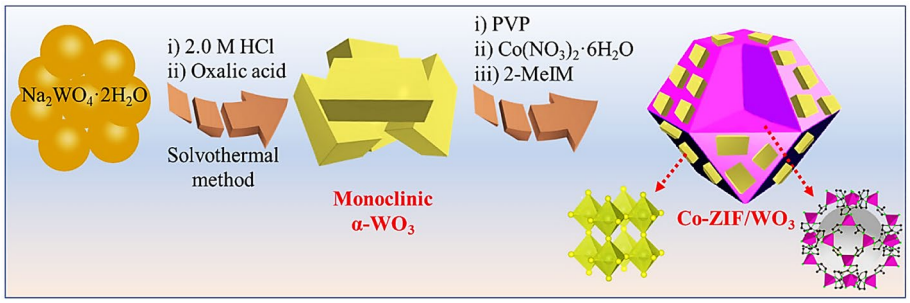

Figure 1. Synthetic strategy for assembly of Co-ZIF/WO_3 heterostructures.

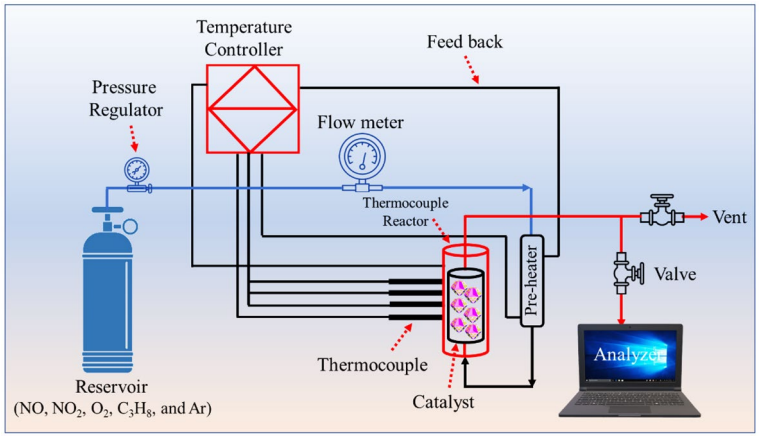

Figure 2. Catalytic reactor for the SCR-NO_x process in the study.

controlled the temperature of the reactor bed over 150–400 ± 1 °C. Gas analysis of the outlet was measured using a sensor probe. Finally, the KANE 940 gas analyzer was conducted to evaluate gases of NO, NO_2, O_2, and CO.

Result and discussion

The crystalline phase of WO_3 and Co-ZIF/WO_3 was assessed using the HA–XRD pattern. As depicted in Fig. 3a, the characteristic diffraction peaks at 22.1°, 23.6°, 24.3°, 34.1°, 41.7°, 49.8°, 54.9°, and 55.8° be indexed α-WO_3 with monoclinic phase and JCPDS Card No. 83-0950[36]. After epitaxial growth of ZIF-67 on surface WO_3, all peaks related to crystal ZIF-67 were revealed in ZIF-67/WO_3 heterostructure[38,39]. Moreover, the chemical groups of the heterostructure were evaluated by FT-IR spectra (Fig. 3b). The peaks at 600–800 cm^{-1} can be ascribed to W–O–W stretching vibration[44], confirming the formation of WO_3. The weak peaks at 460 cm^{-1} revealed the vibration of the Co–N, respectively[45–47] and bands in the range of 800–1300 corresponded to the symmetric and asymmetric stretching of the imidazole rings[47], confirming the formation of ZIF-67 on WO_3 surface. The optical response characteristics of as-obtained nanostructures were evaluated by UV–Vis DRS spectra. As shown in Fig. 3c, the absorption edge of WO_3 was approximately 470 nm, while after epitaxial growth of ZIF-67 on WO_3 exhibited a strong absorption intensity from 350 to 650 nm. Meanwhile, the broad absorption in the UV region (< 400 nm) can be attributed to ligand to metal charge-transfer (LMCT)[36,48], while displaying three absorption peaks at 538, 565, and 590 nm indexed to the $^4A_2(F) \rightarrow {}^4T_1(P)$ transition of Co^{2+} ions in ZIF-67 framework[48–50]. Also, the band-gap values for WO_3 and ZIF-67/WO_3 heterostructure were 2.71 and 1.89 eV, respectively (Fig. 3d), indicating an increase in light absorption capacity. As depicted in Fig. 3e, Co-ZIF and WO_3 revealed positive slopes in the linear regions of the Mott-Schottky plots, illustrating both the nanostructures have n-type semiconductor behavior. Meanwhile, the flat band potential (E_{fb}) derived from Mott-Schottky plots of WO_3 and Co-ZIF were approximately − 0.19 and − 0.37 V (vs Ag/AgCl, pH 7), which are equivalent to − 0.04 V and − 0.23 (vs NHE, pH 0) Eq. (1) [36]. According to (Eqs. (1)–(3) [36] and Mott-Schottky plot, the conduction band (CB) and valence band (VB) of WO_3 were calculated to be − 0.04 eV and 2.67 eV, while those of Co-ZIF were obtained to be − 0.23 eV and 1.66 eV, respectively (Fig. 3f).

$$E_{(Vs.\ NHE,\ pH\ 0)} = E_{(Vs.\ Ag/AgCl,\ pH\ 7)} - 0.0591\left(7 - pH_{electrolyte}\right) + 0.198 \quad (1)$$

$$E_{VB} = E_{CB} + E_g \quad (2)$$

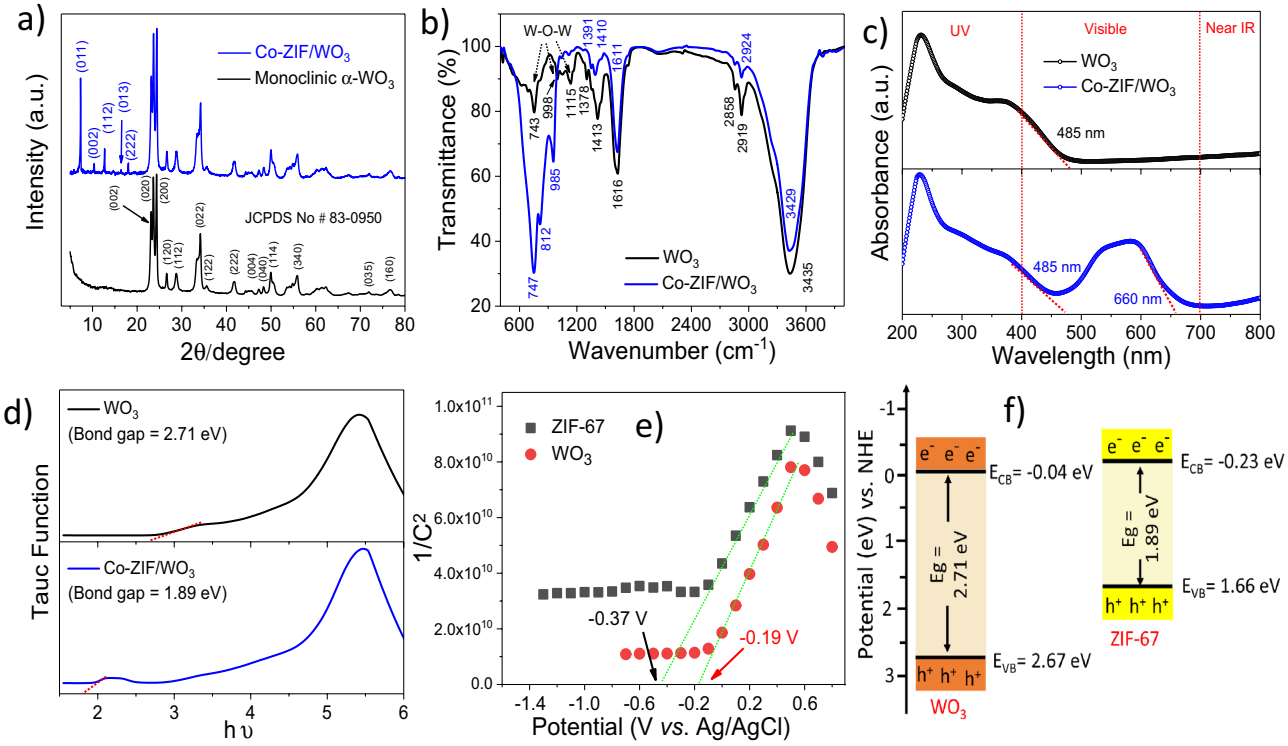

Figure 3. The HA-XRD pattern (**a**), FT-IR spectra (**b**), UV–Vis DRS spectrum (**c**), Tauc plot (**d**), Mott-Schottky plot (**e**), and bandgap structures of obtained nanostructures.

$$E_{CB} = E_{(Ag/AgCl)} + E^{\theta}_{(Ag/AgCl)} + 0.0591\ pH \quad (3)$$

Moreover, N_2 adsorption–desorption isotherm was conducted for the evaluation of the surface area and pore size of Co-ZIF/WO_3 heterostructure. As depicted in Fig. 4a and Table 1, the heterostructure indicated a typical type I isotherm with surface area $S_{BET} = 1061\ m^2/g$ and total pore = 0.35 cm^3/g. Meanwhile, ZIF-67 and WO_3 revealed a typical type II and III isotherms with $S_{BET} = 1420\ m^2/g$ and 16.17 m^2/g, respectively. According to the BJH plot (Fig. 4b), the corresponding pores diameter distributions of the Co-ZIF/WO_3, ZIF-67, and WO_3 were specified at 1.21, 1.23, and 4.69 nm respectively. These microporous structures with larger specific surface areas in Co-ZIF/WO_3 heterostructure can be provided suitable to the adsorption of gases and catalytic activity.

The morphology and structure of the prepared catalysts were evaluated by FESEM, AFM, and TEM. The pure WO_3 exhibited a plate-like structure with a thickness of about 45 nm (Fig. 5a). After the growth of the ZIF-67 on WO_3, these metal oxides were heterogeneously dispersed over the surface of ZIF-67 (Fig. 5b). Meanwhile, the structures and morphology of ZIF-67 and WO_3 about preserved after composition. Also, SEM-mapping (Fig. 5c) and EDS analysis (Fig. S1, ESI) demonstrated the purity and elements corresponding to the heterostructure. Moreover, the presence of WO_3 nanoplates in the core of the proposed heterostructure was not observed with

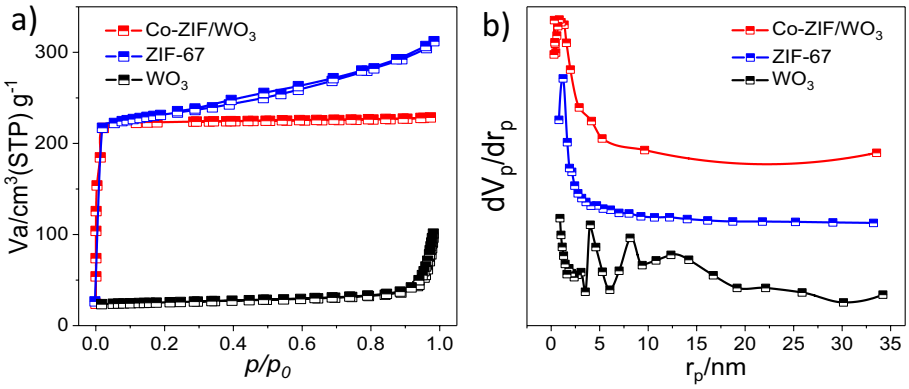

Figure 4. N_2 adsorption–desorption isotherms (**a**) and BJH plot (**b**) for Co-ZIF/WO_3, ZIF-67, and WO_3 nanostructures.

Samples	Textural properties		
	BET (m^2/g)	Pore diameter (nm)	Pore volume (cm^3/g)
WO_3	16.176	4.69	0.119
ZIF-67	1420.34	1.23	0.734
Co-ZIF/WO_3	1061.51	1.21	0.351

Table 1. Textural properties of samples.

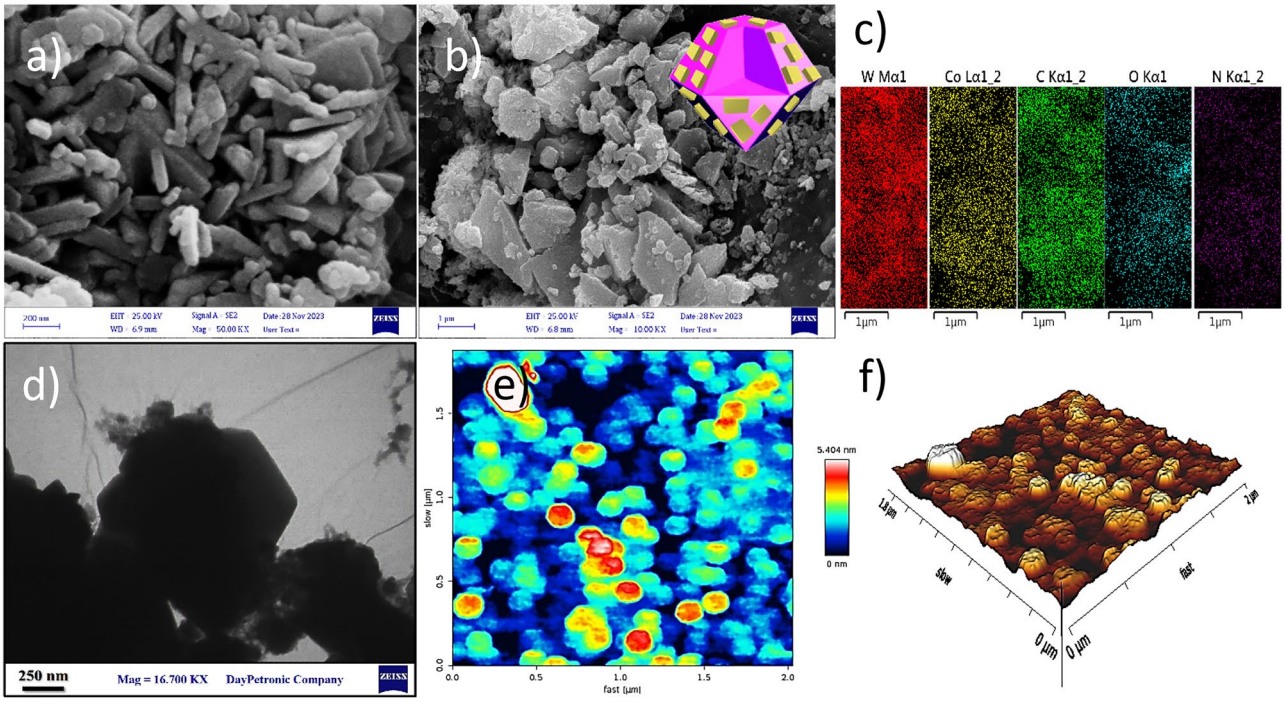

Figure 5. FESEM images of WO_3 (**a**) and Co-ZIF/WO_3 (**b**); FESEM-mapping of Co-ZIF/WO_3 (**c**); TEM image of Co-ZIF/WO_3 (**d**); and 2D AFM and 3D AFM images of Co-ZIF/WO_3 (**e**, **f**).

FESEM images; therefore, the TEM image was conducted to further evaluated the morphology and growth of ZIF-67 with WO_3. As displayed in Fig. 5d, WO_3 nanoplates were observed on the surface of ZIF-67 with rhombic dodecahedral framework morphology. This image further confirmed the formation of Co-ZIF/WO_3 to composite form. Furthermore, AFM analysis indicated surface morphology and roughness of the proposed heterostructure. As depicted in Fig. 5e and f, the arithmetic average roughness (Ra) of Co-ZIF/WO_3 was approximately 150 nm, which appeared in light and dark regions in the 2D and 3D images.

After characterization of the proposed heterostructure, the activity of WO_3, ZIF-67, and Co-ZIF/WO_3 was evaluated on the conversion of NOx to N_2. The total NOx to N_2 conversion curve as a function of reaction temperature for all samples at gas hourly space velocity (GHSV) 51,048 h^{-1}. As depicted in Fig. 6a, all samples reveal a similar trend in NOx reduction efficiency. Meanwhile, all samples have a maximum conversion at 350–400 °C, then activity was decreased. The smallest conversion factor (55%) belongs to WO_3 nanoplates at 400 °C due to not being porous material and having a low specific surface area. Also, the maximum activity occurred for ZIF-67 and Co-ZIF/WO_3 heterostructure with a conversion rate of 62% and 78% at 350 °C, respectively. Therefore, the corresponding maximum transition temperature changes from 50 °C to a lower temperature for ZIF-67 and Co-ZIF/WO_3 heterostructure. Research has revealed that WO_3 is an n-type semiconductor with negligible porous structure, which has the least conversion of NOx into N_2 in comparison to ZIF-67 and Co-ZIF/WO_3. Meanwhile, the ZIF-67 indicated a suitable conversion of NOx into N_2 due to the microporous structure and high surface area (S_{BET} = 1420.34 m^2/g, Table 1 and Fig. S2, ESI). Also, ZIF-67 contains cobalt species that can promote the active site in the SCR-NOx process. Therefore, the composition of WO_3 nanoplates with ZIF-67 microcrystals led to increasing catalytic activity due to interaction and electron transfer facility between the WO_3 and Co species in the Co-ZIF/WO_3. It should be noted that in some additional runs, the mass of prepared nanostructures and GHSV were increased by 20% at the constant reaction temperature. Since no significant changes in turnover were observed at the concentrations of N_2, NO_2, NO, and CO. It was easy to conclude that there was no resistance to mass transport of the gas layer in any of the other experiments. Figure 6b demonstrates the development of the NO_2 concentration in the flue gases as a function of the reaction temperature in the range from 150 to 500 °C for different samples at GHSV 51,048 h^{-1}. An S-shaped curve (decreasing with increasing temperature) was

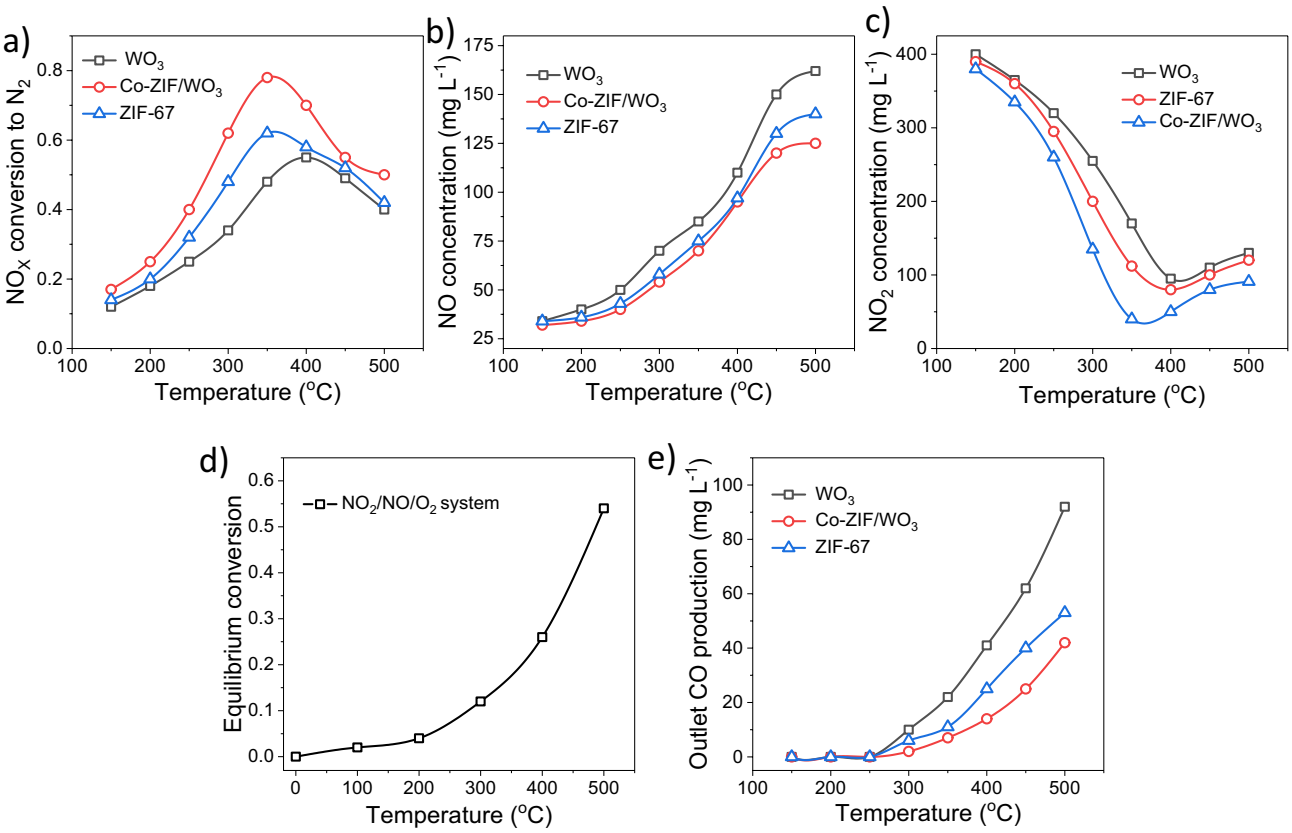

Figure 6. The effect of the reaction temperature and kind of sample on the conversion of NO_x ($NO + NO_2$) into N_2 (**a**), the variation of NO concentration (**b**), the variation of NO_2 concentration in the exhaust gas for different nanostructures (**c**), The equilibrium conversion of NO_2 to NO in the three component system NO_2–NO–O_2 (**d**), and outlet CO concentration of production versus reaction temperature for all samples (**e**).

obtained for each sample. Particularly noteworthy is the variability of the NO concentration in the generated gas depending on the reaction conditions. Also, the change in the NO concentration of the generated gas with the reaction conditions is worth special evaluation. It is known that Mo (650 °C), Ag (160 °C), and stainless steel (450 °C) can catalyze the decomposition reaction of NO_2 to NO. As depicted in Fig. 6b and c, Co-ZIF/WO_3 revealed the lowest NO production concentration and the highest NO_2 concentration reduction. It should be borne in mind that the main nitrogenous reagent in our system is NO_2 due to the decomposition of NO_2 into NO and O_2 at temperatures above 200 °C. As depicted in Fig. 6d, in a three-component system NO_2–NO–O_2 conversions up to 50% are expected at 500 °C due to the residence time of NO_2 species in the reaction system. The findings indicated the formation of CO as an undesired product is inevitable during the NOx reduction in presence of hydrocarbons. As displayed in Fig. 6e, the CO production concentration in Co-ZIF/WO_3 heterostructure is a minimal value compared to WO_3 nanoplates and ZIF-67 microporous (35 ppm at 500 °C). According to our previous studies[26,51], this phenomenon may be related to the non-selective combustion of hydrocarbons (propane) at higher temperatures. Furthermore, the CO generation reaction can activate in Co-ZIF/WO_3 heterostructure channel and does not exclusively take place in the gas phase. However, it is observed that the CO concentration increases with the increase of the reaction temperature, which can be justified by considering the following reactions [Eqs. (4)–(8)][26].

$$2C_3H_8 + 10NO_2 \rightarrow 5N_2 + 6CO_2 + 8H_2O \quad (4)$$

$$C_3H_8 + 2NO + 4O_2 \rightarrow N_2 + 3CO_2 + 4H_2O \quad (5)$$

$$C_3H_8 + 5O_2 \rightarrow 3CO_2 + 4H_2O \quad (6)$$

$$2C_3H_8 + 7O_2 \rightarrow 6CO + 8H_2O \quad (7)$$

$$2NO_2 \leftrightarrow 2NO + O_2 \quad (8)$$

Conclusion

The present study was planned to design and fabricate Co-ZIF/WO_3 heterostructure for NOx reduction emissions. The results obtained from the XRD, FESEM, and TEM indicate the epitaxial growth of ZIF-67 microcrystals onto the WO_3 nanoplates. The catalytic efficiency of the Co-ZIF/WO_3 in terms of NOx reduction is better than that of Co-ZIF, and WO_3. This enhanced activity is attributed to the synergic effect of WO_3 nanoplates loaded into ZIF-67 microcrystals and also the electron transfer facility between them in Co-ZIF/WO3 heterostructures. Moreover, the outlet concentration of CO is lower for Co-ZIF/WO_3 than for ZIF-67, and WO_3, which is an undesirable product in the SCR-NOx-Propane process. Our future efforts will be devoted to designing a new type of nanostructure for the reduction of the CO concentration to near 5 ppm. Finally, our findings provide a feasible strategy for the development of semiconductor-based heterostructures for reducing NOx emissions.

Data availability

The datasets used and/or analyzed in this study are available in the manuscript can be asked from the corresponding author upon request.

Received: 3 October 2023; Accepted: 5 February 2024
Published online: 08 February 2024

References

1. Dickerson, R. R., Anderson, D. C. & Ren, X. On the use of data from commercial NOx analyzers for air pollution studies. *Atmos. Environ.* **214**, 116873 (2019).
2. Azimi, M., Feng, F. & Yang, Y. Air pollution inequality and its sources in SO_2 and NOx emissions among Chinese provinces from 2006 to 2015. *Sustainability* **10**, 367 (2018).
3. Alamgholiloo, H. *et al.* Formation and stabilization of colloidal ultra-small palladium nanoparticles on diamine-modified Cr-MIL-101: Synergic boost to hydrogen production from formic acid. *J. Colloid Interface Sci.* **567**, 126–135 (2020).
4. Alamgholiloo, H., Pesyan, N. N., Mohammadi, R., Rostamnia, S. & Shokouhimehr, M. Synergistic advanced oxidation process for the fast degradation of ciprofloxacin antibiotics using a GO/CuMOF-magnetic ternary nanocomposite. *J. Environ. Chem. Eng.* **9**, 105486 (2021).
5. Dutheil, F. *et al.* Autism spectrum disorder and air pollution: A systematic review and meta-analysis. *Environ. Pollut.* **278**, 116856 (2021).
6. Lu, X., Yao, T., Li, Y., Fung, J. C. & Lau, A. K. Source apportionment and health effect of NOx over the Pearl River Delta region in southern China. *Environ. Pollut.* **212**, 135–146 (2016).
7. Nikokavoura, A. & Trapalis, C. Graphene and g-C_3N_4 based photocatalysts for NOx removal: A review. *Appl. Surf. Sci.* **430**, 18–52 (2018).
8. Amoatey, P., Omidvarborna, H., Baawain, M. S. & Al-Mamun, A. Emissions and exposure assessments of SOX, NOX, PM10/2.5 and trace metals from oil industries: A review study (2000–2018). *Process Saf. Environ. Prot.* **123**, 215–228 (2019).
9. Giannakopoulou, T. *et al.* Tailoring the energy band gap and edges' potentials of g-C3N4/TiO_2 composite photocatalysts for NOx removal. *Chem. Eng. J.* **310**, 571–580 (2017).
10. Ohno, A., Okiyama, Y., Hirose, A. & Fukuhara, K. The position of the nitro group affects the mutagenicity of nitroarenes. *Toxicol. Appl. Pharmacol.* **441**, 115974 (2022).
11. Genc, H. Efficient reductions of various nitroarenes with scrap automobile catalyst and NaBH4. *Catal. Commun.* **67**, 64–67 (2015).
12. Leem, J. H., Kim, S. T. & Kim, H. C. Public-health impact of outdoor air pollution for 2nd air pollution management policy in Seoul metropolitan area. *Korea. Ann. Occup. Environ. Med.* **27**, 1–9 (2015).
13. Shima, M. Health effects of air pollution: A historical review and present status. *Nihon Eiseigaku Zasshi. Jpn. J. Hyg.* **72**, 159–165 (2017).
14. Papailias, I. *et al.* Chemical vs thermal exfoliation of g-C_3N_4 for NOx removal under visible light irradiation. *Appl. Catal. B.* **239**, 16–26 (2018).
15. Wang, J., Yi, H., Tang, X., Zhao, S. & Gao, F. Simultaneous removal of SO_2 and NOx by catalytic adsorption using γ-Al_2O_3 under the irradiation of non-thermal plasma: Competitiveness, kinetic, and equilibrium. *Chem. Eng. J.* **384**, 123334 (2020).
16. Sun, Y., Zwolińska, E. & Chmielewski, A. G. Abatement technologies for high concentrations of NOx and SO_2 removal from exhaust gases: A review. *Crit. Rev. Environ. Sci. Technol.* **46**, 119–142 (2016).
17. Han, L. *et al.* Selective catalytic reduction of NOx with NH_3 by using novel catalysts: State of the art and future prospects. *Chem. Rev.* **119**, 10916–10976 (2019).
18. Abdulrasheed, A. *et al.* Surface modification of activated carbon for adsorption of SO_2 and NOX: A review of existing and emerging technologies. *Sust. Energy Rev.* **94**, 1067–1085 (2018).
19. Sazama, P. *et al.* Unprecedented propane–SCR-NOx activity over template-free synthesized Al-rich Co-BEA* zeolite. *J. Catal.* **332**, 201–211 (2015).
20. Kantcheva, M., Cayirtepe, I., Naydenov, A. & Ivanov, G. FT-IR spectroscopic investigation of the effect of SO_2 on the SCR of NOx with propene over ZrO_2–Nb_2O_5 catalyst. *Catal. Today.* **176**, 437–440 (2011).
21. Gómez-García, M. A., Zimmermann, Y., Pitchon, V. & Kiennemann, A. Multifunctional catalyst for de-NOx processes: The selective reduction of NOx by methane. *Catal. Commun.* **8**, 400–404 (2007).
22. Islam, A. *et al.* Progress in recent sustainable materials for greenhouse gas (NOx and SOx) emission mitigation. *Prog. Mater. Sci.* **132**, 101033 (2022).
23. Li, X. *et al.* Influence of CeO_2 morphology on WO_3/CeO_2 catalyzed NO selective catalytic reduction by NH_3. *J. Energy Inst.* **93**, 1511–1518 (2020).
24. Zhang, W.-B. *et al.* Research progress on NH_3-SCR mechanism of metal-supported zeolite catalysts. *J. Fuel Chem. Technol.* **49**, 1294–1315 (2021).
25. Lee, K., Kosaka, H., Sato, S., Yokoi, T. & Choi, B. Effect of Cu content and zeolite framework of n-C_4H_{10}-SCR catalysts on de-NOx performances. *Chem. Eng. Sci.* **203**, 28–42 (2019).
26. Ghasemian, N., Falamaki, C., Kalbasi, M. & Khosravi, M. Enhancement of the catalytic performance of H-clinoptilolite in propane–SCR–NOx process through controlled dealumination. *Chem. Eng. Sci.* **252**, 112–119 (2014).
27. Berndt, H., Schütze, F.-W., Richter, M., Sowade, T. & Grünert, W. Selective catalytic reduction of NO under lean conditions by methane and propane over indium/cerium-promoted zeolites. *Appl. Catal. B.* **40**, 51–67 (2003).
28. Struzhko, V., Orlyk, S., Myroniuk, T. & Ilyin, V. Synthesis and properties of new catalytic systems based on zirconium dioxide and pentasils for process of NOx selective catalytic reduction by hydrocarbons. *Sci. Bases Prepar. Heterogen. Catal.* **143**, 425–433 (2002).

29. Anstrom, M., Topsøe, N.-Y. & Dumesic, J. Density functional theory studies of mechanistic aspects of the SCR reaction on vanadium oxide catalysts. *J. Catal.* **213**, 115–125 (2003).
30. Lee, K., Choi, B., Kim, C., Lee, C. & Oh, K. De-NOx characteristics of HC-SCR system employing combined Ag/Al_2O_3 and CuSn/ZSM-5 catalyst. *J. Ind. Eng. Chem.* **93**, 461–475 (2021).
31. Yang, G. *et al.* Promotion effect and mechanism of the addition of Mo on the enhanced low temperature SCR of NOx by NH_3 over MnOx/γ-Al_2O_3 catalysts. *Appl. Catal. B.* **245**, 743–752 (2019).
32. Zhao, Y. *et al.* NH_3-selective catalytic reduction performance of a new type of Cu@ ZIF-7 catalyst. *AIP Adv.* **12**, 025113 (2022).
33. Alamgholiloo, H., Pesyan, N. N. & Marjani, A. P. Visible-light-responsive Z-scheme α-Fe_2O_3/SWCNT/NH2-MIL-125 heterojunction for boosted photodegradation of ofloxacin. *Sep. Purif. Technol.* **305**, 122442 (2023).
34. Alamgholiloo, H. *et al.* Facile fabrication of Z-scheme TiO_2/ZnO@ MCM-41 heterojunctions nanostructures for photodegradation and bioactivity performance. *J. Mol. Liq.* **364**, 119990 (2022).
35. Sepehrmansourie, H., Alamgholiloo, H., Pesyan, N. N. & Zolfigol, M. A. A MOF-on-MOF strategy to construct double Z-scheme heterojunction for high-performance photocatalytic degradation. *Appl. Catal. B.* **321**, 122082 (2023).
36. Nazari, S., Asgari, E., Sheikhmohammadi, A., Mokhtari, S. A. & Alamgholiloo, H. Visible-light-driven photocatalytic activity of WO_3/ZIF-67 S-scheme heterojunction for upgrading degradation of oxytetracycline. *J. Environ. Chem. Eng.* **11**, 110393 (2023).
37. Alamgholiloo, H. *et al.* Architecture of bimetallic-MOF/silicate derived Co/NC@ mSiO_2 as peroxymonosulfate activator for highly efficient ciprofloxacin degradation. *Sep. Purif. Technol.* **300**, 121911 (2022).
38. Hashemzadeh, B. *et al.* Degradation of ciprofloxacin using hematite/MOF nanocomposite as a heterogeneous fenton-like catalyst: A comparison of composite and core–shell structures. *Chemosphere* **281**, 130970 (2021).
39. Alamgholiloo, H. *et al.* A facile strategy for designing core-shell nanocomposite of ZIF-67/Fe_3O_4: A novel insight into ciprofloxacin removal from wastewater. *Process Saf. Environ. Prot.* **147**, 392–404 (2021).
40. Li, S., Wang, F., Xie, Z., Ng, D. & Shen, B. A novel core-shell structured Fe@ CeO_2-ZIF-8 catalyst for the reduction of NO by CO. *J. Catal.* **421**, 240–251 (2023).
41. Wu, T., Guo, R.-T., Li, C.-F., You, Y.-H. & Pan, W.-G. Recent advances in core-shell structured catalysts for low-temperature NH3-SCR of NOx. *Chemosphere* **333**, 138942 (2023).
42. Bai, Y. *et al.* Co_3O_4@ PC derived from ZIF-67 as an efficient catalyst for the selective catalytic reduction of NOx with NH_3 at low temperature. *Chem. Eng. J.* **361**, 703–712 (2019).
43. Ma, J. *et al.* Topochemical preparation of WO_3 nanoplates through precursor H2WO4 and their gas-sensing performances. *J. Phys. Chem. C.* **115**, 18157–18163 (2011).
44. Mohamed, H. H. Rationally designed Fe_2O_3/GO/WO_3 Z-Scheme photocatalyst for enhanced solar light photocatalytic water remediation. *J. Photochem. Photobiol. A.* **378**, 74–84 (2019).
45. Li, H. *et al.* Co nanoparticles encapsulated in N-doped carbon nanofibers as bifunctional catalysts for rechargeable Zn-air battery. *Appl. Surf. Sci.* **478**, 560–566 (2019).
46. Wang, F. *et al.* Enhanced catalytic sulfamethoxazole degradation via peroxymonosulfate activation over amorphous CoSx@ SiO_2 nanocages derived from ZIF-67. *J. Hazard. Mater.* **423**, 126998 (2022).
47. Zhou, K. *et al.* Characterization and properties of Zn/Co zeolitic imidazolate frameworks vs ZIF-8 and ZIF-67. *J. Mater. Chem. A.* **5**, 952–957 (2017).
48. Pattengale, B. *et al.* Exceptionally long-lived charge separated state in zeolitic imidazolate framework: Implication for photocatalytic applications. *J. Am. Chem. Soc.* **138**, 8072–8075 (2016).
49. Li, H. *et al.* Efficient oxidation of ethylbenzene catalyzed by cobalt zeolitic imidazolate framework ZIF-67 and NHPI. *J. Energy Chem.* **23**, 742–746 (2014).
50. Zhang, Y. & Jin, Z. Boosting photocatalytic hydrogen evolution achieved by NiSx coupled with g-C_3N_4@ ZIF-67 heterojunction. *J. Phys. Chem. C.* **123**, 18248–18263 (2019).
51. Zinatloo-Ajabshir, S., Ghasemian, N., Mousavi-Kamazani, M. & Salavati-Niasari, M. Effect of zirconia on improving NOx reduction efficiency of $Nd_2Zr_2O_7$ nanostructure fabricated by a new, facile and green sonochemical approach. *Ultrason. Sonochem.* **71**, 105376 (2021).

Acknowledgements

This research was supported by Department of Environmental Health Engineering, School of Health, Khoy University of Medical Sciences (Grant number: 400000015 and Ethical Code: IR.KHOY.REC.1400.008).

Author contributions

H.A.: Investigation in preparation of the catalyst, write the manuscript; E.A.: Review & editing and supervisor; A.S.: Formal analysis and supervisor; N.G.: Investigation in NOx reduction; B.H.: Methodology; and H.N.: Review & editing. All the authors agree to publish this article.

Competing interests

The authors declare no competing interests.

Additional information

Supplementary Information The online version contains supplementary material available at https://doi.org/10.1038/s41598-024-53805-7.

Correspondence and requests for materials should be addressed to E.A., A.S. or N.G.